Modeling the Constitutive Response of Bimodal Metals

S.P. JOSHI, K.T. RAMESH, B.Q. HAN, and E.J. LAVERNIA

The mechanical response of metals with a bimodal grain-size distribution is modeled using the secant Mori–Tanaka (M-T) mean-field approach. The actual microstructure of bimodal metals involves a grain size distribution in the ultrafine and coarse regimes; the model approximates this in terms of two phases with distinct grain sizes and with specific volume fractions. The model is applied to two bimodal materials: the Al-5083 alloys of Lavernia *et al*. and the Cu of Wang *et al.* In both the materials, the predictions agree well with the experiments. In the bimodal Al alloy, the effect of extrusion on the anisotropy in yield strength and flow behavior is also addressed. Finally, based on the model predictions, an empirical expression of the Voce form is proposed to describe the overall flow behavior of both bimodal metals.

I. INTRODUCTION

BULK nanostructured (NS, grain size (d) < 100 nm) and ultrafine-grained (UFG, $d < 500$ nm) metals possess superior mechanical strength over their conventional coarse-grained (CG, $d \gg 1$ μm) counterparts; this is attributed to the increased resistance to dislocation generation and movement with grain size refinement.[1] Grain size refinement is of significant interest in load bearing components as it creates attractive opportunities to design lighter and stronger structures.[2] For example, aluminum and its alloys are important candidates for grain-refinement-based strengthening due to their potential utility in a wide range of engineering areas such as automotive and aerospace components (as matrix material in composites), structural and nonstructural applications in construction, packaging, *etc*. However, it has been observed that as the hardness increases with grain refinement, most materials typically suffer from loss of ductility, causing failure at small strains; this is attributed to several causes including artifacts from processing, plastic instability in tension, *etc*.[3,4,5] To overcome this limitation, several strategies have been demonstrated ranging from innovative processing routes to tailoring the grain structure.[5,6,7] A promising approach demonstrated by Wang *et al*. on UFG copper[8] was to use a nonuniform grain size distribution in order to delay plastic instability (which is a primary cause of low ductility) and to improve strain hardening. In an earlier study,[9] a nanostructured aluminum alloy with an intrinsic bimodal microstructure was generated *via* consolidation of cryomilled nanostructured aluminum powders using hot isostatic pressing and hot extrusion. The bimodal material from this study showed an excellent combination of strength and ductility. Inspired by this finding, the processing of cryomilled aluminum alloys with a bimodal microstructure was successfully performed *via* consolidation of a mixture of nanostructured powders with unmilled coarse-grained powders to achieve strengthening as well as ductility.[10] The bimodal microstructure comprises a combination of ultrafine grains (~200 nm) and relatively coarser grains (CG-Al, 500 to 1000 nm), which is the main focus of the present work. A detailed review of the UFG and the bimodal Al alloys produced by cryomilling and their mechanical behaviors is presented in the work of Lavernia and co-workers.[10,11] The addition of a CG fraction to the UFG material leads to improved ductility, although it also decreases the yield strength in comparison to a fully cryomilled UFG alloy. The success of bimodal alloys relies on finding optimal fractions and arrangements of the ultrafine and coarse grains together with additional strengthening mechanisms (dispersions, plastic work hardening, *etc*.) such that the compromise of the yield strength is minimal.

The recent focus of efforts on bimodal metals is on the experimental characterization of the effects of processing routes on their structure and properties.[8,12–15] Witkin *et al*.[16] investigated the intrinsic bimodal microstructure developed during hot isostatic pressing and the microstructural evolution during subsequent thermomechanical treatments of cryomilled Al alloys. Additionally, mechanical responses of UFG Al alloys at low loading rates[17] and elevated temperatures[18] have been studied to identify the active deformation mechanisms. However, comparatively little work has focused on developing constitutive models to predict the mechanical behavior of these alloys. In a previous study, finite element (FE)–based approaches such as the unit cell model were used to study the behavior of bimodal materials.[8,19]

An alternative to the FE approach is to use explicit analytical expressions based on the Mori–Tanaka (M-T) mean-field concept;[20] this approach is fast and can predict the mechanical response over the entire range of the inclusion shapes and volume fractions. In the modified version of the theory presented by Weng,[21] the secant approach allows the elasto-plastic representation of both phases. The two phases are represented in a matrix-inclusion topology and the secant approach models the weakening constraint of the matrix as the macroscopic stress or strain increases. The method has shown promise in predicting the stress-strain behavior of dual-phase steels[21,22] and metal matrix composites with elastic inclusions.[23] In this paper, we adopt the secant M-T approach to model the constitutive response of bimodal metals.

In Section II, we consider bimodal Al-5083 alloy[13] as the model case. Using the secant approach, the longitudinal

S.P. JOSHI, Postdoctoral Fellow, is with the Center for Advanced Metallic and Ceramic Systems (CAMCS) and the Department of Mechanical Engineering, The Johns Hopkins University, Baltimore, MD 21218. Contact e-mail: spjoshi@jhu.edu K.T. RAMESH, Professor, is with the Department of Mechanical Engineering, The Johns Hopkins University. B.Q. HAN, Associate Project Scientist, and E.J. LAVERNIA, Professor, are with the Department of Chemical Engineering and Materials Science, University of California, Davis, CA 95616.

Manuscript submitted February 9, 2006.

(extrusion direction) and transverse stress-strain behaviors are obtained. The overall mechanical behavior of the bimodal Al alloy is calculated using the stress-strain responses of the two "phases" idealized as a 200-nm UFG phase and a 1-μm CG phase. The effect of matrix-inclusion topology on the flow stress is studied. The model is then employed to predict the response of bimodal Cu,[6] produced using a different processing technique (*viz.* severe plastic deformation), but with a similar grain size distribution. The numerical results for the bimodal Al-5083 and Cu are presented and compared to the corresponding experimental observations. Finally, a simple expression of the Voce form is proposed that describes the overall flow behavior for both the materials.

The theoretical framework for bimodal metals is given in the Appendix so that the form of the model is clear. For a detailed description of the secant approach, the reader is referred to Weng.[21] An essential modification to Weng's model is the empirical function employed in describing the stress–plastic strain behavior of the individual phases. A characteristic feature of NS and UFG metals is the rapid strain hardening behavior followed by near perfect plasticity. We describe this behavior using the Voce equation instead of the Ludwig equation,[21] as it better represents the aforementioned saturation behavior.

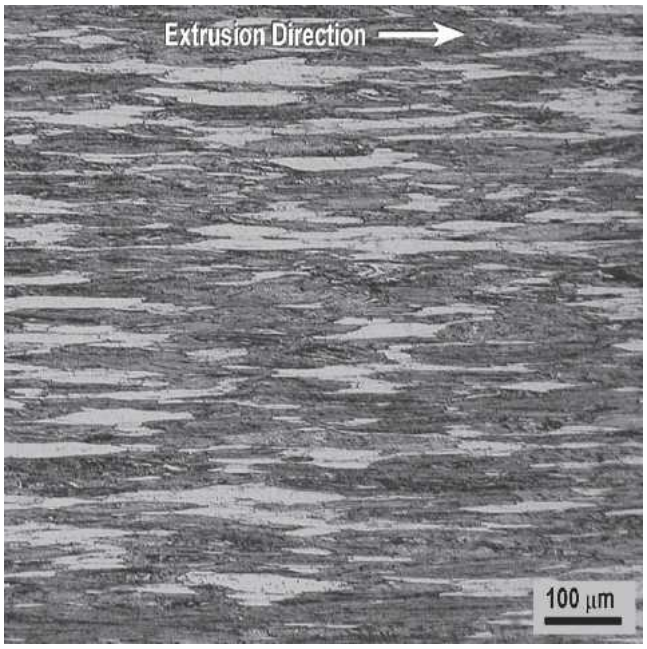

Fig. 1—Optical micrograph of bimodal Al-5083 alloy in the longitudinal direction with 30 pct CG-Al volume fraction.

II. MODELING RESULTS AND COMPARISON WITH EXPERIMENTS

A. *Bimodal Al-5083*

Bimodal Al-5083 alloys are made of cryomilled nanocrystalline Al-5083 powders blended with a specified volume fraction of unmilled Al-5083 powders. The mixture is consolidated at ambient temperature (*via* cold isostatic pressing) and extruded (in bar form) at a high temperature. The final microstructure shows a grain size (d) distribution with a significant fraction (nearly 60 to 70 pct) at approximately 200 nm, designated the ultrafine-grained phase (UFG). Furthermore, depending on the amount of unmilled Al-5083 added during blending, the remaining grain-size distribution ranges between 500 and 1000 nm, designated the coarse-grained (CG) Al 5083 phase. Figure 1 shows a typical microstructure of bimodal Al-5083 with 30 pct CG phase in the longitudinal direction: both UFG (dark regions) and the CG (light regions) phases are elongated along the extrusion direction. Compression results of the bimodal 5083 Al alloys with 0, 15, 30, and 50 pct volume fractions of CG-Al are available[13] in both the longitudinal and transverse directions at a strain rate of 10^{-3} s^{-1}. Although the real microstructure has a distribution in the grain size, the model presented in this article approximates this as explicitly bimodal, with two distinct grain sizes ($d_{\text{ufg-Al}} = 200$ nm and $d_{cg\text{-Al}} = 1$ μm). Their corresponding stress-strain behaviors are used to compute the overall mechanical response.

The elastic modulus (E) and the Poisson's ratio (ν) for UFG-Al 5083 are 70 GPa and 0.33, respectively. As discussed in Section I, the stress-strain response of the individual phases is described using the Voce equation (Eq. [A1] in the Appendix). Using regression analysis, we fit the Voce parameters to the experimental stress-strain data for the UFG-Al 5083 given in Reference 13. The fitting parameters are the saturation stress ($\sigma_s = 710$ MPa), initial yield stress ($\sigma_y = 580$ MPa), and the characteristic strain ($\varepsilon_c = 0.0084$).

In order to proceed with the numerical calculations, the stress-strain curves for both the phases are required. However, no experimental data are presently available for the CG-Al phase within the bimodal alloy. Therefore, we estimate the response of this material by modifying the known response of conventional Al-5083 to account for the effects of grain size (using the Hall–Petch relation, $\sigma_y = \sigma_0 + k_y d^{-1/2}$) and prior plastic work. The elastic modulus and the Poisson's ratio for the CG-Al phase are essentially the same as that of the UFG-Al phase. The reference yield strength (σ_0) for conventional Al-5083 is 130 MPa. For Al-Mg alloys, the Hall–Petch coefficient (k_y) varies between 0.12 and 0.30 MPa m$^{1/2}$ depending on the chemical composition.[11] We assume $k_y = 0.13$ MPa m$^{1/2}$, which corresponds to conventional Al-5Mg alloys.[24] The estimated yield strength after grain-size refinement for this CG-Al is then 260 MPa. Further, significant plastic work is done on the material as it undergoes extrusion during sample preparation. Typical extrusion ratios used in Reference 11 correspond to a plastic strain of about 1.9. Although the work hardening of the virgin (*i.e.*, at room temperature and low strains) CG-Al could be expected to be high (similar to that of conventional Al-5083), dynamic recovery at high temperature during extrusion (~823 K) would limit this behavior, resulting in lower saturation stress that occurs at strains smaller than those expected for conventional Al-5083. In the present case, accurate description of stress saturation at high temperature for CG-Al 5083 is unavailable; we assume that the difference between the saturation stress (σ_s) and the initial yield stress (σ_0) of extruded CG-Al is the same as that of the UFG phase, *i.e.*, 130 MPa. Given that the initial yield stress of CG-Al is 260 MPa, the

plastic work would elevate the yield stress level to 390 MPa. As the CG-phase experiences large plastic work during extrusion, we assume that it follows the work hardening behavior of the UFG phase. We use these parameters as inputs to compute the overall response of the composite and compare this with the measured response in the longitudinal direction.

1. *Longitudinal direction*

Using the secant M-T approach and the material description outlined in the preceding paragraphs, the overall stress-strain behavior of bimodal Al-5083 is predicted for 0 pct, 15 pct, 30 pct, and 50 pct volume fractions of CG-Al (Figure 2). The model predictions agree with the experimental results except for the 15 pct volume fraction. The model predicts that the yield strength drops as the CG-Al volume fraction is increased from 0 to 15 pct. The experimental observation, however, shows marginally stronger performance for the ''15 pct'' material than the ''0 pct'' material, which seems unusual. An examination of the histograms in the reference[13] reveals that the 15 pct CG-Al alloy has a grain size distribution that is not very different from that of the 0 pct CG-Al. Less than 1 pct of the coarse-grained volume fraction in the 15 pct material has a grain size of about 1 μm, while the remainder is distributed in the 300- to 800-nm range; as a consequence, the experimental results on the 0 and 15 pct materials are similar. The model considers that the entire 15 pct volume fraction of CG material has a grain size of 1 μm; as expected, the predicted response is softer, and thus is different from the experimental results. At higher volume fractions, the 1-μm grain size dominates the coarse-grained microstructure in the real materials and correspondingly the predictions compare better with the experiments. The model also accurately captures the initial rapid strain hardening behavior followed by near zero strain hardening. From a microstructural viewpoint, the presence of the brief strain-hardening region is attributed to the existence of pre-existing subgrain structure due to cryomilling and extrusion.[25] The subsequent near-perfect plastic deformation is attributed to the lack of dislocation accumulation in cryomilled Al alloys. Because of the high stacking fault energy in Al alloys, dislocations can easily cross-slip and annihilate by reacting with other dislocations, leading to dynamic recovery.[26,27] In addition, dislocations can emit from the boundary on one side of a grain and annihilate at the other side because of the short slip distance in nanostructured materials.[28,29] The net result is the rapid change in stress, which is captured by the Voce equation that is based on saturation of stress.

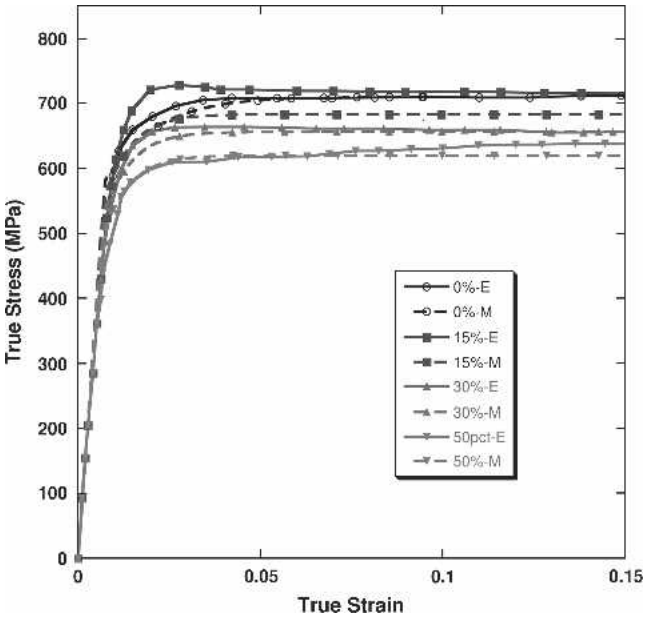

Fig. 2—Comparison of longitudinal model (M, dashed lines) and experimental (E, marked lines) stress-strain curves for different percentage volume fractions of CG-Al.

The inclusion phase is assumed to be spherical in shape in the model. Due to the extrusion process, the grains in the inclusion phase are actually elongated in the extrusion direction. We have extended the model to account for prolate inclusions (results not presented here) and found that this does not lead to appreciable changes in the stress levels, as the material properties of the two phases do not differ dramatically.

2. *Transverse direction*

The experimental results[13] for compression in the direction normal to the axis of extrusion indicate two important features. First, the yield strengths for different CG-Al volume fractions are lower in the transverse direction than in the longitudinal direction. Note that this anisotropy is not seen for the 0 pct CG-Al case, indicating that the softer CG-Al sustains most of the additional (initial) plastic deformation during extrusion. Second, the ductility of the material is less; this is attributed to shear failure at small strains.[13] The anisotropy in the yield strengths and strain hardening in the longitudinal and the transverse directions may be attributed to the larger initial plastic deformation experienced by the softer CG-Al phase (as compared to harder UFG-Al) in the extrusion direction than in the transverse direction. Because of the smaller initial plastic work in the transverse direction, the CG-Al phase in the model is assumed to retain the high strain hardening prevalent in the conventional Al-5083 at small plastic strains. The Voce parameters in the transverse direction are taken as $\sigma_s = 450$ MPa and $\varepsilon_c = 0.081$, which are obtained for conventional Al-5083 at low initial plastic work.[30] The grain size effect is included as previously discussed. The inclusion phase in the model is assumed spherical, as both the phases appear equiaxed in the transverse direction. Using this description, the numerical predictions correlate well with the experimental observations (Figure 3). Unlike the longitudinal direction, the transverse experiments show a consistent decrease in the yield strength with increasing CG-Al volume fraction. It is interesting to note that the coarse grain-size distribution effect in the 0 and 15 pct cases mentioned in the results for the longitudinal compression does not appear to be significant in the transverse direction. A possible reason is that although the grain size distribution for the two cases is similar, they possess different mechanical behaviors in the transverse direction as a result of the processing route. In the 0 pct case, the entire material is cryomilled, whereas the 15 pct material has an unmilled fraction in

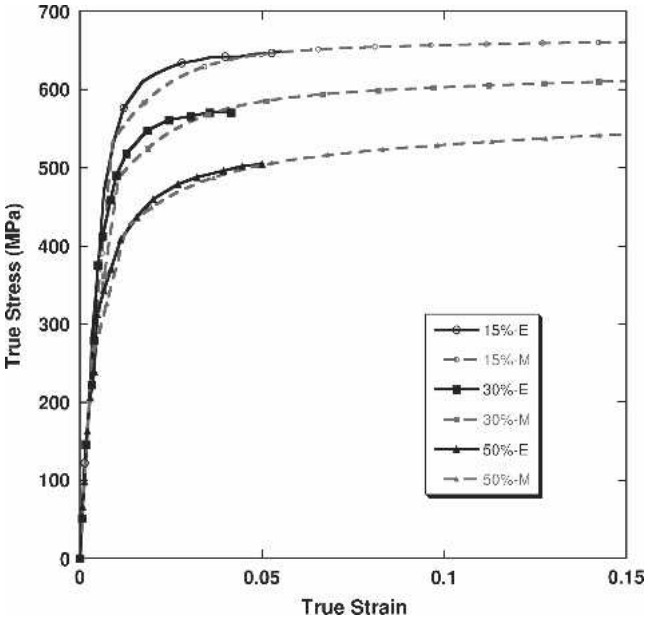

Fig. 3—Comparison of transverse model (M, dashed lines) and experimental (E, marked lines) stress-strain curves for different percentage volume fractions of CG-Al.

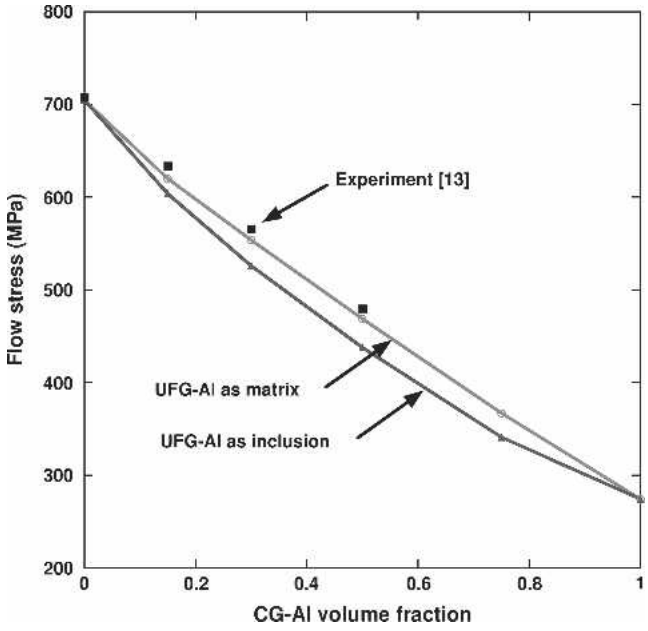

Fig. 4—Variation in the transverse directional flow stress at 2 pct macroscopic plastic strain as a function of volume fraction of CG-Al.

its distribution. Consequently, owing to low initial plastic work in the transverse direction, the presence of soft unmilled fraction in the 15 pct material leads to lower strength despite having a grain size distribution that is similar to the 0 pct material.

3. *Effect of volume fraction*

The predicted effect of CG-Al volume fraction on the flow stress is compared with the flow stress in the experiments at 2 pct macroscopic plastic strain (Figure 4) for the transverse direction. Experimental observations show that the transverse flow stress depends linearly on the CG volume fraction. From a mechanics viewpoint, it is indeed remarkable that the material follows a rule-of-mixture as such a dependence is not expected at high volume fractions of the reinforcing phase (>10 pct). To address this behavior, we investigate the effect of matrix-inclusion topology on the macroscopic response. Our model shows that the flow stress in the transverse direction is different based on whether CG-Al is treated as a matrix phase or as an inclusion phase. When the UFG-Al is the matrix, the flow stress decreases linearly at the rate of about 4.2 MPa per percent increase in the CG-Al volume fraction; this is consistent with the experimental results (~4 to 4.5 MPa per pct CG-Al). However, when the CG-Al is considered as the matrix, the flow stress shows a nonlinear dependence on the CG-Al volume fraction, which is not seen in the experiments. This indicates that even at these high CG-Al volume fractions, the UFG-Al phase effectively serves as the matrix. In the longitudinal direction, the predicted flow stress at 2 pct macroscopic plastic strain is observed to decrease linearly (not shown in the figure) with an increase in the CG-Al volume fraction, which is qualitatively consistent with the observations in the previous study.[13] Further, the same flow stress is predicted irrespective of whether the CG-Al serves as the matrix or as an inclusion.

In view of the volume fraction effects in the longitudinal and transverse directions, we find that in both cases the linear approximation seems to be reasonable when the UFG-Al is considered to be the matrix material (even at the relatively high volume fractions of the CG phase of nearly 50 pct).

Although it is not obvious in Figure 3, the model does indicate increased strain hardening in the transverse direction with the CG-Al volume fraction. This suggests that the material should exhibit delayed necking under tensile loading. Presently, we do not have comparable experimental data for this material. To this end, we predict the onset of tensile instability from our model results using the Considére criterion ($(d\sigma/d\varepsilon)_{\dot{\varepsilon}} \leq \sigma$, where σ and ε and are the true stress and strain corresponding to a tension test conducted at a fixed strain rate, $\dot{\varepsilon}$). As seen from Figure 5, the model predicts that the onset of tensile necking increases almost linearly with increasing CG-Al volume fraction. Increased strain hardening is expected to improve tensile ductility as it delays the plastic instability. We note that for all the CG-Al volume fractions considered, the predicted values of necking strain are in the vicinity of the strains at which the material fails in shear during compression experiments.[13] We do not currently have an explanation for this correspondence between observed compressive failure strain and predicted tensile necking strain.

While the model predicts increased necking strain with CG volume fraction for the transverse direction, it cannot predict the same for longitudinal Al-5083. This is because in the longitudinal direction the strain hardening response chosen for the CG phase is the same as that of the UFG phase. The experimental results also do not indicate strong dependence of strain hardening on the CG volume fraction. As discussed in the preceding sections, the coupled effect of initial plastic straining and temperature during extrusion causing anisotropy in the yield strength and strain hardening of the softer CG phase. Therefore, in the optimal design of

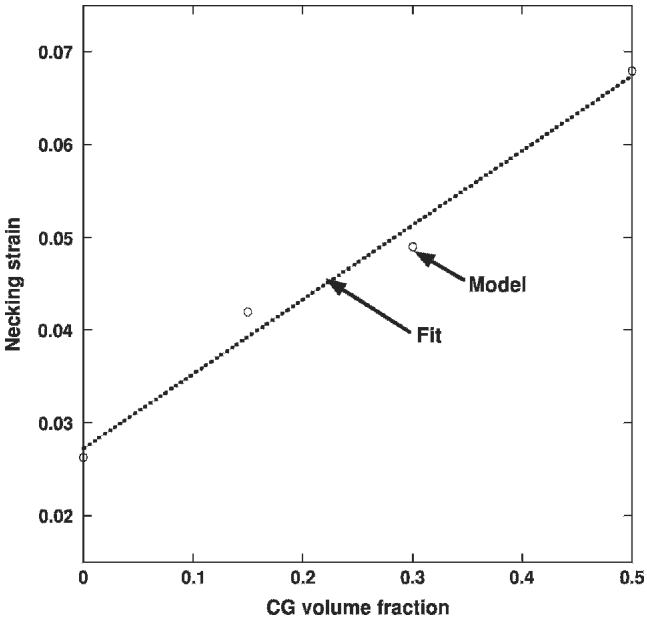

Fig. 5—Onset of tensile instability predicted by the model as a function of coarse grain volume fraction for transverse Al-5083 based on Considere criterion. (The dotted line is a linear fit to the predictions.)

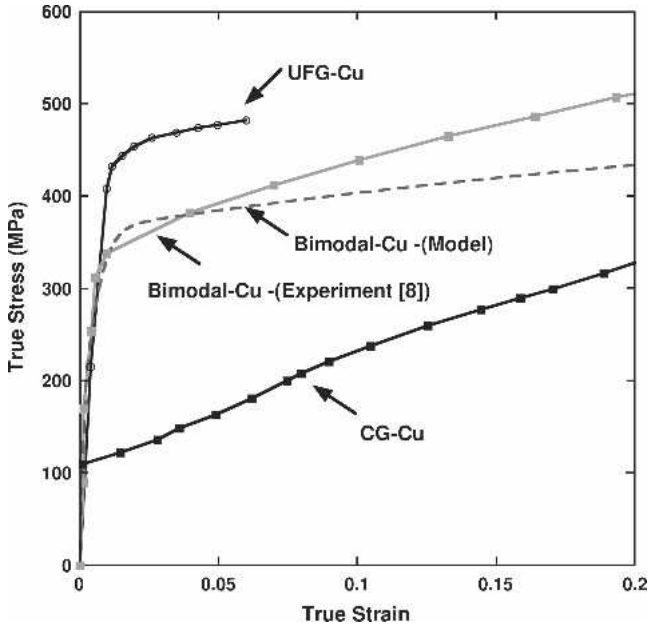

Fig. 6—Comparison of the experimental (symbols) and numerically predicted (plain) stress-strain curves for bimodal Cu with 25 pct CG volume fraction.

bimodal metals, the process parameters could be important design variables; for example, one would evaluate optimal values of extrusion ratio and temperature such that the CG phase in bimodal metals contributing to ductility remains relatively free of initial strain.

B. *Bimodal Copper*

Given the success of the model in predicting the behavior of bimodal Al-5083, we employ the method to model the response of the bimodal Cu considered by Wang *et al.*[8] In contrast to the bimodal Al-5083, which was produced by cryomilling, blending, and extrusion, Wang *et al.*[8] produced UFG-Cu using equal channel angular pressing (ECAP). They subjected the ECAP-Cu to a unique thermo-mechanical treatment (cryorolling followed by heat treatment at 200 °C for 3 minutes causing partial recrystallization) to produce a bimodal microstructure in UFG-Cu. The coarse grains ($d \sim 1$ to 3 μm) constitute about 25 pct volume fraction, while the remaining fraction has a grain size ranging from a few tens to hundreds of nanometers. Tensile tests showed significant improvement in strength and ductility as compared to their CG and UFG counterparts, respectively. We use the experimental data for UFG and CG phases from their tests as input to the model; the true stress-strain curves are calculated from the engineering stress-strain curves for the UFG (curve D[8]) and the CG (curve A[8]) phases. It appears that curve A represents the stress-strain response of conventional Cu with grain size much larger than the largest grain size in the bimodal material. Assuming an average grain size of 2.0 μm and $k_y = 0.1$ MPa $m^{1/2}$,[31] the yield strength for the CG fraction should be 110 MPa. As noted by Huang and Hansen,[32] the strain hardening is not affected by grain size; hence, we assume the same strain hardening behavior as observed for conventional coarse-grained Cu in the reference.[8] The elastic modulus and the Poisson's ratio for both phases are 100 GPa and 0.34, respectively. The Voce parameters are as follows:

$$\text{UFG-Cu: } \sigma_y = 270 \text{ MPa}, \sigma_s = 470 \text{ MPa}, \varepsilon_c = 0.0036$$
$$\text{CG-Cu: } \sigma_y = 110 \text{ MPa}, \sigma_s = 968 \text{ MPa}, \varepsilon_c = 0.675$$

Note that the preceding parameters were fitted to the experimental data up to the strain at which the Considére criterion is reached; *i.e.*, up to strains of 0.06 and 0.38 for the UFG and CG phases, respectively. Figure 6 compares the overall response predicted by the model with the experimental result from Wang *et al.*[8] The model predicts the macroscopic yielding and the initial strain hardening response of the bimodal material. However, as the strain increases beyond 0.05, the predicted strain hardening response deviates from the real response. Wang *et al.*[8] report that at larger strains the material exhibits higher strain hardening for several reasons including twinning observed in large sized grains and high strain gradients between the UFG and the CG phases; these higher order effects arising from the interaction are not included in the model. However, the model predictions appear reasonable up to strains of ~0.1.

C. *Empirical Constitutive Functions*

Application of this model to materials design is most easily accomplished if simple expressions are available for the overall response. We present simple expressions for the macroscopic flow stress of bimodal materials that represent our numerical results. In the case of Al-5083 alloy, the anisotropy in the overall response could be modeled using a Hill-type anisotropic yield function.[33] However, such a description requires at least three independent tests (two uniaxial, one biaxial/shear) to extract the unknown anisotropy coefficients (*e.g.*, for a plane state

of stress), and these coefficients would be a function of the CG-Al volume fraction. At this point, we cannot describe the anisotropic coefficients unambiguously as only uniaxial test data are available. As an alternative, we decouple the responses in the two loading directions as they coincide with the orthogonal material directions. The macroscopic response can then be defined independently in each direction assuming two separate yield behaviors. Thus, at a given CG volume fraction, Eq. [1] represents a Voce-type expression that predicts the flow behavior of the composite:

$$\bar{\sigma}_f = \bar{\sigma}_s - (\bar{\sigma}_s - \bar{\sigma}_y) \exp\left(\frac{\bar{\varepsilon}_p}{\bar{\varepsilon}_c}\right) \quad [1]$$

To remain consistent with the predictions, we express the parameters $\bar{\sigma}_s, \bar{\sigma}_y$, and $\bar{\varepsilon}_c$ as linear functions of the CG volume fraction (f_{cg}) where the coefficients depend on the material characteristics of the two phases:

$$\bar{\sigma}_s = c_1 + c_2 f_{cg} \quad [2a]$$

$$\bar{\sigma}_y = c_3 + c_4 f_{cg} \quad [2b]$$

$$\bar{\varepsilon}_c = c_5 + c_6 f_{cg} \quad [2c]$$

Table I indicates the coefficients (c_1 through c_6) in Eqs. [2a] through [c] for bimodal Al-5083 and Cu. The coefficients are valid for CG volume fractions up to about 0.3. Figure 7 shows good agreement among the experimental flow stresses, those predicted by the model, and the empirical function (Eqs. [1] and [2]) for both the materials. Thus, the strength and the hardening parameters for bimodal Al alloy follow an effective rule of mixtures. Note that the coefficients for bimodal Cu are intended to provide reasonable estimates of the flow behavior only at plastic strains up to about 6 pct.

Table I. Values for the Coefficients in Equation [2a–c] for Bimodal Materials

	c_1	c_2	c_3	c_4	c_5	c_6
Al-5083 longitudinal	710	−180	580	−218	0.0084	−0.0086
Al-5083 transverse	710	−329	580	−356	0.0084	0.065
Cu	470	−261	270	−510	0.0036	0.03

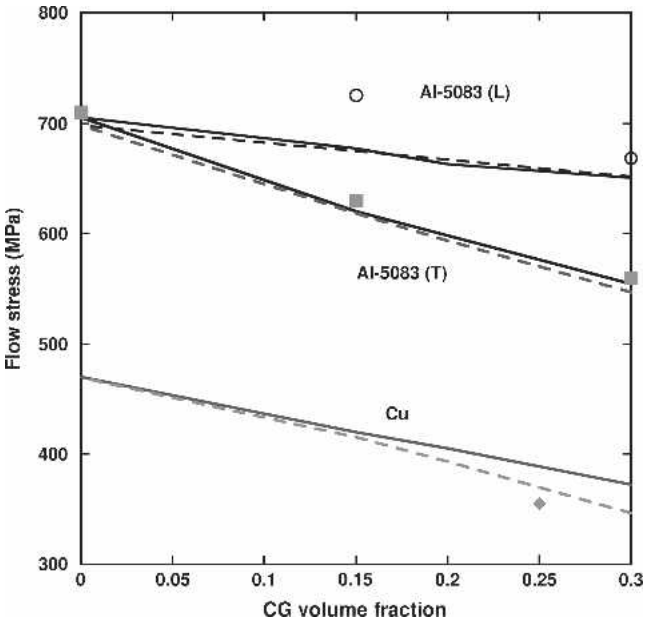

Fig. 7—Comparison of the predictions based on Eq. [2] (dashed lines) with those obtained from the experiments (symbols) and the model (solid lines) for Al-5083 (longitudinal (L) and transverse (T)) and Cu. The values correspond to 2 pct macroscopic plastic strain.

III. SUMMARY

We adopt the secant M-T mean-field approach to simulate the mechanical behavior of bimodal metals. The model approximates the actual grain size distribution in the UFG and CG regimes in terms of two phases with specific volume fractions, each having distinct grain sizes. For bimodal Al-5083, in the absence of experimental data for the CG phase, the stress-strain response is derived using the effects of grain size and plastic work and temperature during extrusion. Under these assumptions, the predicted results for the composite in both the longitudinal and transverse directions compare well with their corresponding experimental results. The effect of high temperature in conjunction with high initial plastic work due to extrusion is highlighted as a plausible explanation for the observed anisotropy in the yield strength and the flow behavior of the alloy in the two directions. The flow stress in the extrusion direction follows the rule of mixtures irrespective of which phase serves as the matrix. In the transverse direction, however, the flow stress predictions deviate from linearity if the softer phase is considered as the matrix, while the experimental data indicates linearity. Thus, in view of the numerical and experimental results, it appears that the UFG-Al serves as an effective matrix even at these high volume fractions of CG-Al (up to 50 pct). In the bimodal Cu case, the model predicts the macroscopic yield accurately and also the strain hardening at low strains. At higher strains, it underestimates the hardening response possibly because both the effect of twinning and high strain gradients that arise as the interaction between the two phases are not modeled. Finally, an empirical constitutive function of the Voce form is proposed to describe the flow behavior of both the bimodal materials. The flow stress parameters in the empirical expression follow a linear dependence on the CG volume fraction providing a quick and reasonable estimate of the flow stress for the bimodal metals studied in this work.

ACKNOWLEDGMENTS

This work was performed under the auspices of the Center for Advanced Metallic and Ceramic Systems (CAMCS) at the Johns Hopkins University and supported by the United States Army Research Laboratory through ARMAC-RTP Cooperative Agreement No. DAAD19-01-2-0003. SPJ and KTR acknowledge the financial support

provided by the Army Research Laboratory through Grant No. DAAL01-96-2-0047. The partial support of this work (BQH and EJL) from the Office of Naval Research, under Contract No. N00014-03-1-0149, is gratefully acknowledged.

APPENDIX

In the secant approach presented by Weng,[21] the behavior of each phase and the composite is described in a deformation theory framework. The matrix phase is referred to as phase 1 and the inclusion phase is referred to as phase 2. Using the Voce form to describe the flow behavior of the rth phase, we have

$$\sigma^{(r)} = \sigma_s^{(r)} - \left(\sigma_s^{(r)} - \sigma_y^{(r)}\right) e^{\left(\frac{-\varepsilon_p^{(r)}}{\varepsilon_c^{(r)}}\right)} \qquad [A1]$$

where $\sigma_y^{(r)}, \sigma_s^{(r)}$, $\varepsilon_p^{(r)}$, and ε_c^r are the initial yield stress, saturation stress, plastic strain, and the characteristic strain for the rth phase that are determined from the experimental stress-strain curves for each phase.

Under proportional loading, both phases deform elastically until the yield stress of one of the phases is reached. The dilatational and the deviatoric components of the composite stresses and strains are connected by[21]

$$\bar{\sigma}_{kk} = 3\bar{\kappa}^s \bar{\varepsilon}_{kk} \qquad [A2]$$

$$\bar{\sigma}'_{ij} = 2\bar{\mu}^s \bar{\varepsilon}'_{ij} - \frac{2\mu_1^s f_2 \mu_2}{f_1 \beta_1^s (\mu_2 - \mu_1^s) + \mu_1^s} (\varepsilon_p)_{ij}^{(2)} \qquad [A3]$$

where the $(\bar{\kappa}^s)$and $(\bar{\mu}^s)$ are the secant bulk and shear moduli of the composite, respectively;[21] f_r is the volume fraction of the rth phase; and β_1^s is the deviatoric component of the Eshelby tensor.

If the matrix yields first, the dilatational and the deviatoric macroscopic stress components in the composite in terms of corresponding prescribed macroscopic strain components are obtained from Eqs. [A2] and [A3] by setting $(\varepsilon_p)_{ij}^{(2)} = 0$. Alternatively, the inclusion phase may yield first and the macroscopic stress state must now be computed at a prescribed equivalent plastic strain in the inclusion $(\varepsilon_p^{*(2)})$. The equivalent plastic strain in the composite is obtained as

$$\bar{\varepsilon}_p^* = f_2 b_2 \varepsilon_p^{*(2)} \qquad [A4]$$

where b_2 is the average elastic stress concentration factor in the inclusion. The effective stress in the composite is given as

$$\bar{\sigma}^* = \frac{1}{b_2}\left[\sigma_s^{(2)} - \left(\sigma_s^{(2)} - \sigma_y^{(2)}\right) e^{\left(\frac{-\varepsilon_p^{*(2)}}{\varepsilon_c^{(2)}}\right)} + 3\mu_1(1-\beta_1) f_1 b_2 \varepsilon_p^{*(2)}\right] \qquad [A5]$$

Finally, when both phases deform plastically, the following expressions are solved simultaneously:

$$b_1^s \bar{\sigma}^* + 3\mu_1^s (1-\beta_1^s) f_2 b_2^s \varepsilon_p^{*(2)} = \sigma_s^{(1)} - \left(\sigma_s^{(1)} - \sigma_y^{(1)}\right) e^{\left(\frac{-\varepsilon_p^{*(1)}}{\varepsilon_c^{(1)}}\right)} \qquad [A6]$$

$$b_2^s \bar{\sigma}^* - 3\mu_1^s (1-\beta_1^s) f_1 b_2^s \varepsilon_p^{*(2)} = \sigma_s^{(2)} - \left(\sigma_s^{(2)} - \sigma_y^{(2)}\right) e^{\left(\frac{-\varepsilon_p^{*(2)}}{\varepsilon_c^{(2)}}\right)} \qquad [A7]$$

where b_r^s is the stress concentration factor for the rth phase based on the secant parameters. At a prescribed effective plastic strain in the matrix $(\varepsilon_p^{*(1)})$, Eqs. [A6] and [A7] are used to obtain the effective inclusion plastic strain$(\varepsilon_p^{*(2)})$ and the effective stress in the composite $(\bar{\sigma}^*)$. The composite plastic strain components are obtained using the Hencky flow rule, and finally, the macroscopic strains in the composite are evaluated from Eqs. [A2] and [A3].

In Eqs. [A1] through [A7], the dilatational and deviatoric components of the Eshelby tensor are defined in terms of the secant parameters of the matrix as

$$\alpha_1^s = \frac{1}{3}\left(\frac{1+\nu_1^s}{1-\nu_1^s}\right) \text{ and } \beta_1^s = \frac{2}{15}\left(\frac{4-5\nu_1^s}{1-\nu_1^s}\right) \qquad [A8]$$

In Eqs. [A6] and [A7], the deviatoric components of the secant stress concentration factors for the two phases are defined as

$$b_1^s = \frac{\beta_1^s(\mu_2 - \mu_1^s) + \mu_1^s}{[(f_2 + f_1\beta_1^s)(\mu_2 - \mu_1^s) + \mu_1^s]} \text{ and } b_2^s = \frac{\mu_2}{[(f_2 + f_1\beta_1^s)(\mu_2 - \mu_1^s) + \mu_1^s]} \qquad [A9]$$

The average elastic deviatoric stress concentration factors in Eqs. [A4] and [A5] can be calculated from Eq. [A9] by using the elastic shear modulus and the Eshelby term for phase 1.

REFERENCES

1. R.Z. Valiev: *Nature*, 2002, vol. 419, pp. 887-89.
2. R.Z. Valiev: *Nature Mater.*, 2004, vol. 3, pp. 511-16.
3. E. Ma: *Scripta Mater.*, 2003, vol. 49, pp. 663-68.
4. Q. Wei, S. Cheng, K.T. Ramesh, and E. Ma: *Mater. Sci. Eng. A*, 2004, vol. 381, pp. 71-79.
5. C.C. Koch: *Scripta Mater.*, 2003, vol. 49, pp. 657-62.
6. Y.M. Wang and E. Ma: *Acta Mater.*, 2004, vol. 52, pp. 1699-709.
7. R.Z. Valiev, R.V. Alexandrov, Y.T. Zhu, and T.C. Lowe: *J. Mater. Res.*, 2002, vol. 17, pp. 5-8.
8. Y. Wang, M.-W. Chen, F. Zhou, and E. Ma: *Nature*, 2002, vol. 419, pp. 912-15.
9. V.L. Tellkamp, A. Melmed, and E.J. Lavernia: *Metall. Mater. Trans. A*, 2001, vol. 32A, pp. 2335-43.
10. B.Q. Han, E.J. Lavernia, and F.A. Mohammed: *Rev. Adv. Mater. Sci*, 2005, vol. 9, pp. 1-16.
11. D. Witkin and E.J. Lavernia: *Progr. Mater. Sci.*, 2005, vol. 51, pp. 1-60.

12. D. Witkin, Z. Lee, R. Rodriguez, S. Nutt, and E.J. Lavernia: *Scripta Mater.*, 2003, vol. 49, pp. 297-302.
13. B.Q. Han, Z. Lee, D. Witkin, S. Nutt, and E.J. Lavernia: *Metall. Mater. Trans. A*, 2005, vol. 36A, pp. 957-65.
14. S. Billard, J.P. Fondere, B. Bacroix, and G.F. Dillard: *Acta Mater.*, 2006, vol. 54, pp. 411-21.
15. S. Billard, E. Meslin, G.F. Dirras, J.P. Fondere, and B. Bacroix: *J. Mater. Sci. Technol.*, 2004, vol. 20, pp. 1-5.
16. D. Witkin, B.Q. Han, and E.J. Lavernia: *J. Mater. Res.*, 2005, vol. 20, pp. 2117-26.
17. G.J. Fan, G.Y. Wang, H. Choo, P.K. Liaw, Y.S. Park, B.Q. Han, and E.J. Lavernia: *Scripta Mater.*, 2005, vol. 52, pp. 929-33.
18. D. Witkin, B.Q. Han, and E.J. Lavernia: *J. Mater. Eng. Performance*, 2005, vol. 14, pp. 519-27.
19. R.Q. Ye, B.Q. Han, and E.J. Lavernia: *Metall. Mater. Trans. A*, 2005, vol. 36A, pp. 1833-40.
20. T. Mori and K. Tanaka: *Acta Metall.*, 1973, vol. 21, pp. 571-74.
21. G.J. Weng: *J. Mech. Phys. Solids*, 1990, vol. 38, pp. 419-41.
22. Rudiono and Tomota: *Acta Mater.*, 1997, vol. 45, pp. 1923-29.
23. C.W. Nan and D.R. Clarke: *Acta Mater.*, 1996, vol. 44, pp. 3801-11.
24. D.J. Lloyd and S.A. Court: *Mater. Sci. Technol.*, 2003, vol. 19, pp. 1349-54.
25. S.L. Semiatin, K.V. Jata, M.D. Uchic, P.B. Berbon, D.E. Matejczyk, and C.C. Bampton: *Scripta Mater.*, 2001, vol. 44, pp. 395-400.
26. R. Kral: *Phys. Status Solidi A*, 1996, vol. 157, pp. 255-63.
27. D. Kuhlmann-Wilsdorf: *Phil. Mag. A*, 1999, vol. 79, pp. 955-1008.
28. Y.T. Zhu and T.G.J. Langdon: *Met*, 2004, pp. 58-63.
29. Y.T. Zhu and X. Liao: *Nature Mater.*, 2004, vol. 31, pp. 351-52.
30. B.Q. Han, F.A. Mohammed, and E.J. Lavernia: *J. Mater. Sci.*, 2003, vol. 38, pp. 3319-24.
31. T.H. Courtney: *Mechanical Behavior of Materials,* McGraw-Hill, New York, NY, 2000.
32. X. Huang and N. Hansen: *Mater. Sci. Eng., A*, 2004, vols. 387–389, pp. 186-90.
33. R. Hill: *The Mathematical Theory of Plasticity*, Oxford University Press, Oxford, United Kingdom, 1986.